Electronic Supplementary Information (ESI)

Magnetic beads extraction on a rotating microfluidic platform

Jakob Wimmer,[a,b] Carole Planchette,[c] Gerhard A. Holzapfel[a,d]
and Theresa Rienmüller*[a]
[a] Institute of Biomechanics, Graz University of Technology, Austria
[b] Erba Technologies Austria GmbH, Graz, Austria [c] Institute of Fluid Mechanics and Heat Transfer, Graz University of Technology, Austria
[d] Department of Structural Engineering, Norwegian University of Science and Technology (NTNU), Trondheim, Norway
* E-mail: theresa.rienmueller@tugraz.at

This ESI includes: (1) a description of the lab-on-a-disc prototype, including exploded view of the disc; (2) details on the absorption measurements, comprising the disc design used for the calibration as well as the calibration curve itself; (3) the magnetic properties of the beads, including their magnetization curve; (4) a comparison demonstrating the effects of cooperative bead motion with the relative importance of magnetophoresis-induced convection and bead aggregation into chains; and (5) an investigation of the influence of the magnetic field on the particle slip velocity, together with maps of the magnetic flux density for each magnet configuration and for different distances between the magnet ring and the disc.

Lab-on-a-disc prototype

Fig. S 1 shows the structure of the lab-on-a-disc prototype. The device consists of a multilayer stack of PMMA and PSA sheets arranged in the following order: (i) PMMA, (ii) PSA, (iii) PMMA, (iv) PSA, (v) PMMA (exploded view). Chambers and connecting channels are clearly visible in the exploded view.

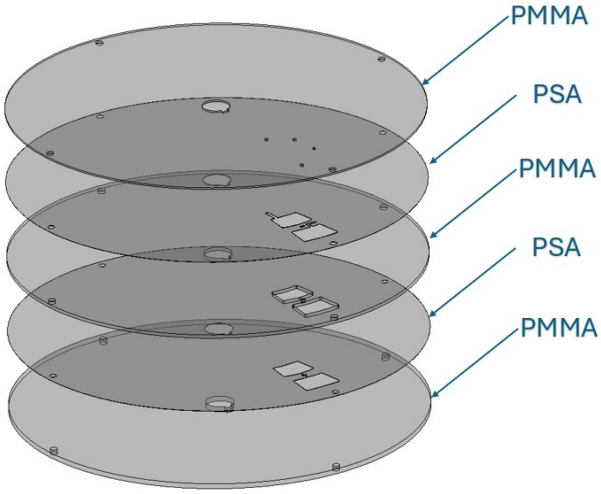

Fig. S 1: Structure of the lab-on-a-disc prototype (exploded view). The diameter of the disc is $12\,\mathrm{cm}$.

Absorption measurements

Fig. S 2 shows the disc used for calibration, with 11 chambers whose magnetic bead dilutions varied linearly from $0\,\mathrm{g/L}$ to $1\,\mathrm{g/L}$. Each chamber contained $60\,\mathrm{\mu L}$ of bead solution. These chambers were imaged under identical light and camera settings to compute absorbance per chamber.

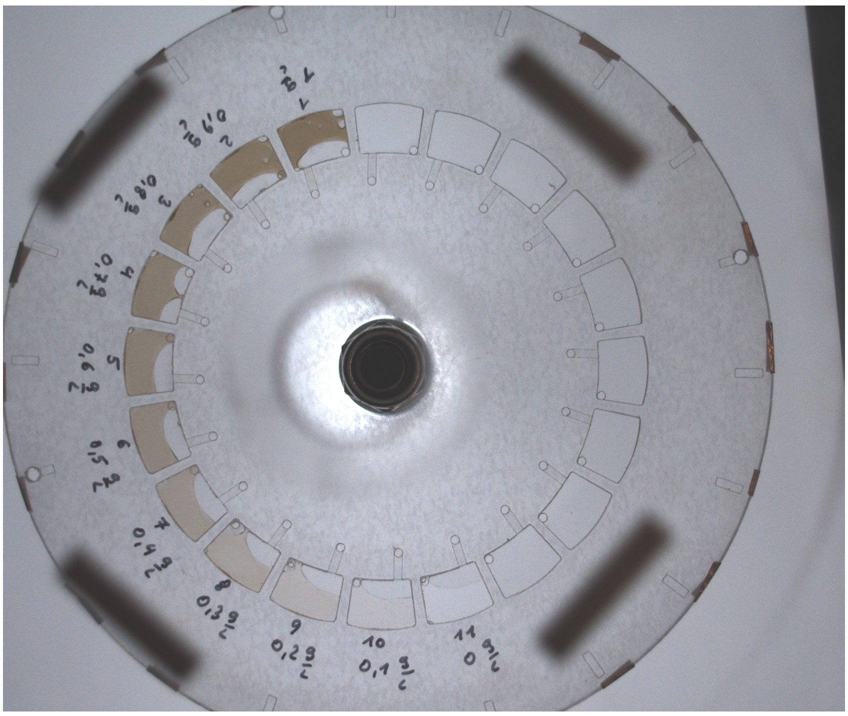

Fig. S 2: Disc containing 11 magnetic bead dilutions ($0\,\mathrm{g/L}$ to $1\,\mathrm{g/L}$

Fig. S 3 displays the calibration curve obtained from the 11 dilutions (Fig. S 2) with the measured absorbance versus bead concentration and a fitted line ($y = 0.189x$) with $R^2 = 0.998$.

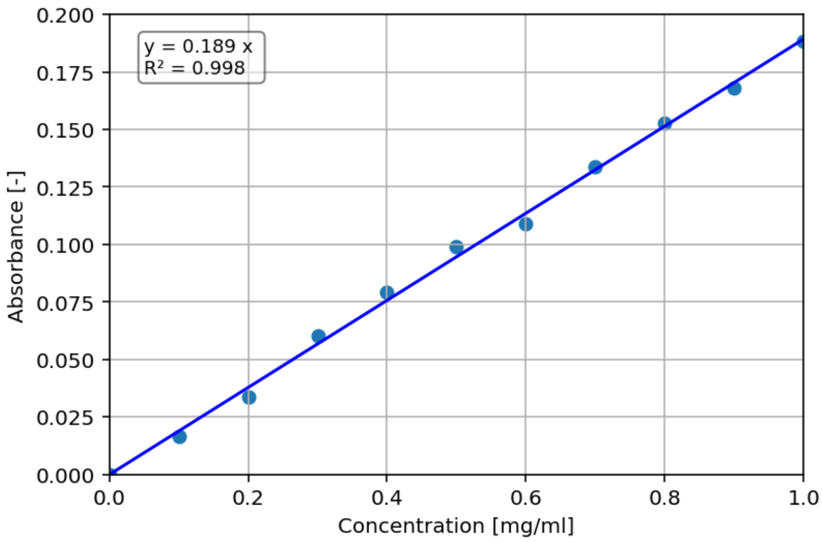

Fig. S 3: Calibration curve for bead concentration (Beer–Lambert validation)

This validates the applicability of the Beer–Lambert law for the concentration range used and the reliability of the image analysis-based absorbance measurement.

Magnetic properties of the beads

Fig. S 4 reproduces the magnetization curve, M versus B, for Dynabeads M270 published by Grob *et al.* [1], where M denotes the magnetization and $B = |\mathbf{B}|$ is the flux density. These data were used to extract parameters required for simulations, including the iron content and density of the beads. Superparamagnetic nanoparticles exhibit randomly oriented magnetic moments at room temperature, so that a bulk sample without an applied field shows negligible magnetization, remanence, and hysteresis. At an applied magnetic flux density $|\mathbf{B}|$, the magnetic energy $\mu|\mathbf{B}|$ competes with thermal energy $k_\mathrm{B}T$: at small fields, thermal agitation dominates, and the moments remain largely random, whereas increasing $|\mathbf{B}|$ gradually aligns the moments until magnetization saturates. captures this behavior compactly. The bulk magnetization can be written as

$$M(|\mathbf{B}|) = M_\mathrm{sat}\mathcal{L}(\alpha|\mathbf{B}|), \tag{1}$$

where M_sat is the saturation magnetization and the Langevin function is

$$\mathcal{L}(x) = \coth(x) - \frac{1}{x}. \tag{2}$$

The Langevin parameter α measures the ratio of magnetic to thermal energy and was determined by Fig. S4, [2, 1].

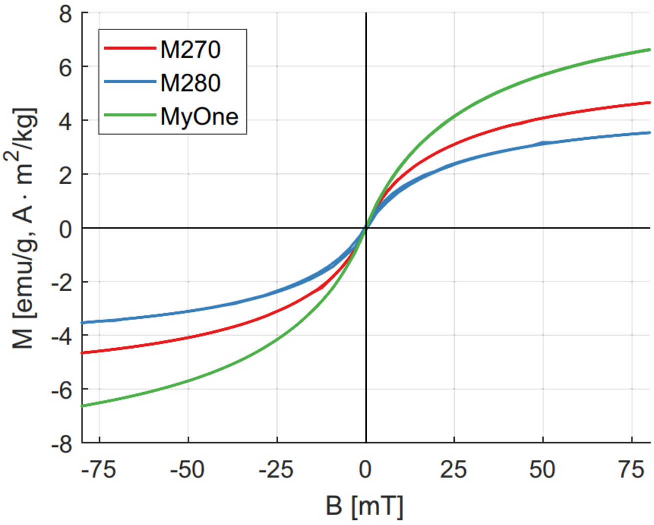

Fig. S 4: Magnetization curve (M versus B) for Dynabeads M270, [1].

Effects of cooperative bead movements

Fig. S 5 shows three collection rate curves from simulations with configuration 1 of the permanent magnet setup: (i) the full model (magnetophoresis-induced convection and particle aggregation into chains), (ii) the model without convection, and (iii) the model without convection and without aggregation. As predicted, the full model shows faster collection kinetics than the other models.

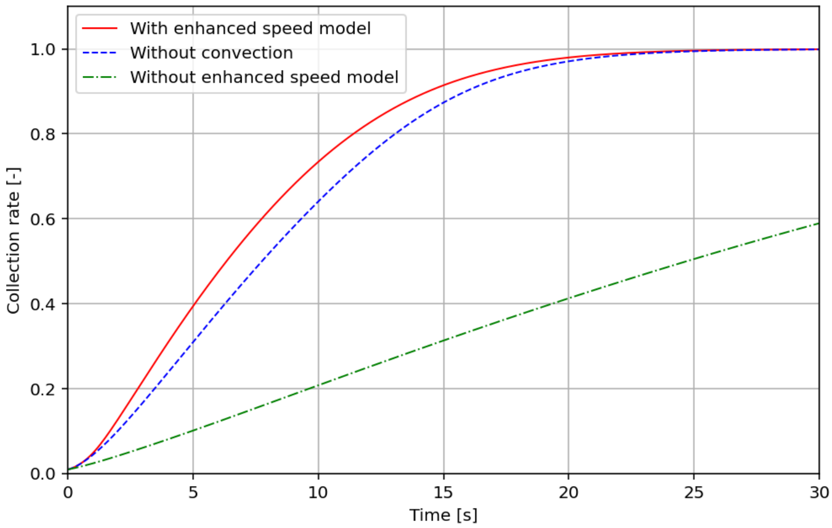

Fig. S 5: Comparison of simulated collection rates: full model versus model without convection versus no convection and no aggregation.

Effects of magnetic field

Figs. S 6 and S 7 show the simulated slip velocity of the particles and magnetic flux density in the collection chamber cross section (yz plane) as described in Fig. 5 of the manuscript, where the collection site is on the top right corner of the cross section. Fig. S 6 shows these fields for each of the permanent magnet configurations, whereas Fig. S 7 shows these fields for the permanent magnet configuration 1 at different distances from the fluid. Each image shows an individual scale bar, which must be considered when comparing the different simulation parameters.

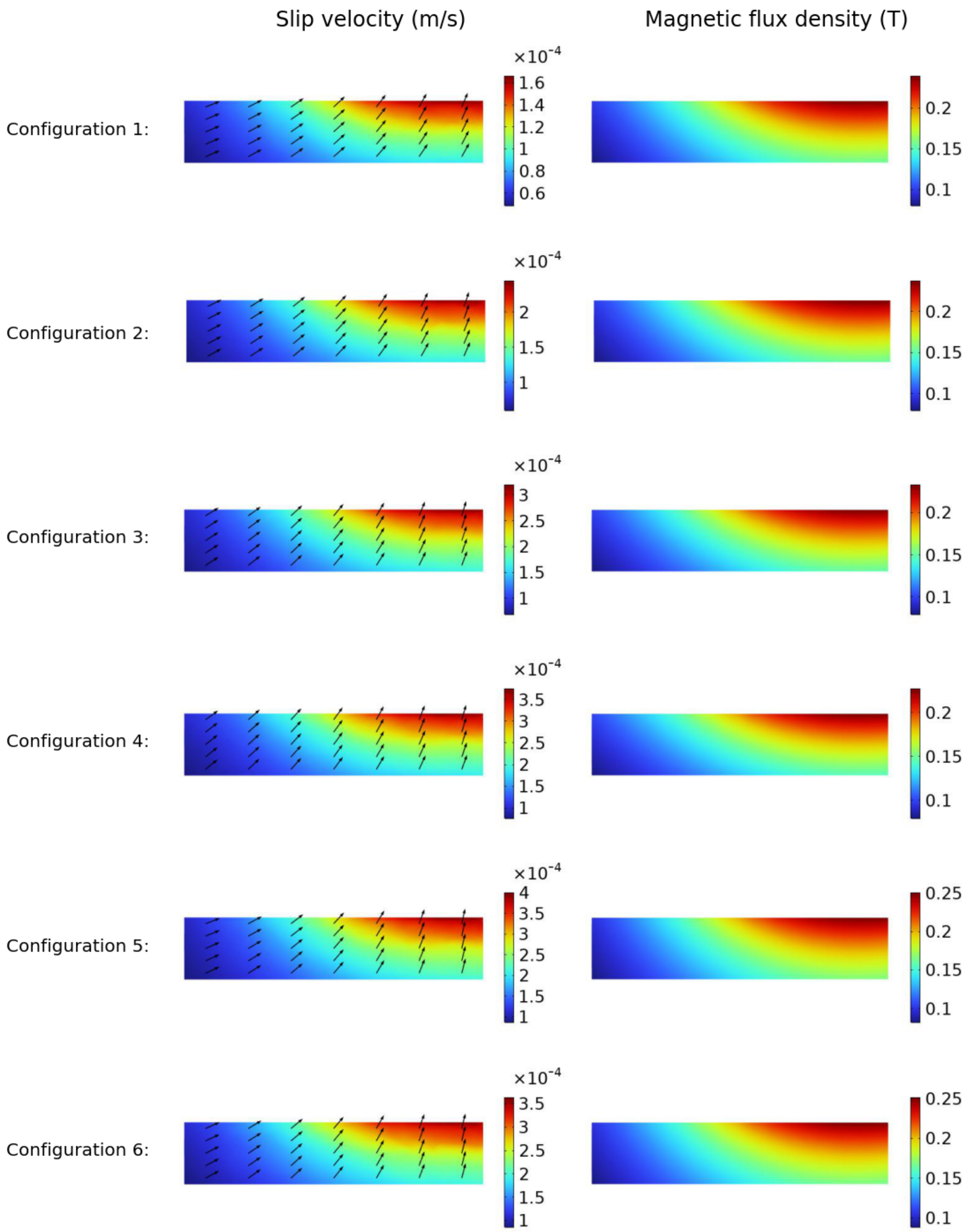

Fig. S 6: Left: Slip velocities and right: magnetic flux densities in the collection chamber cross section for different permanent magnet configurations.

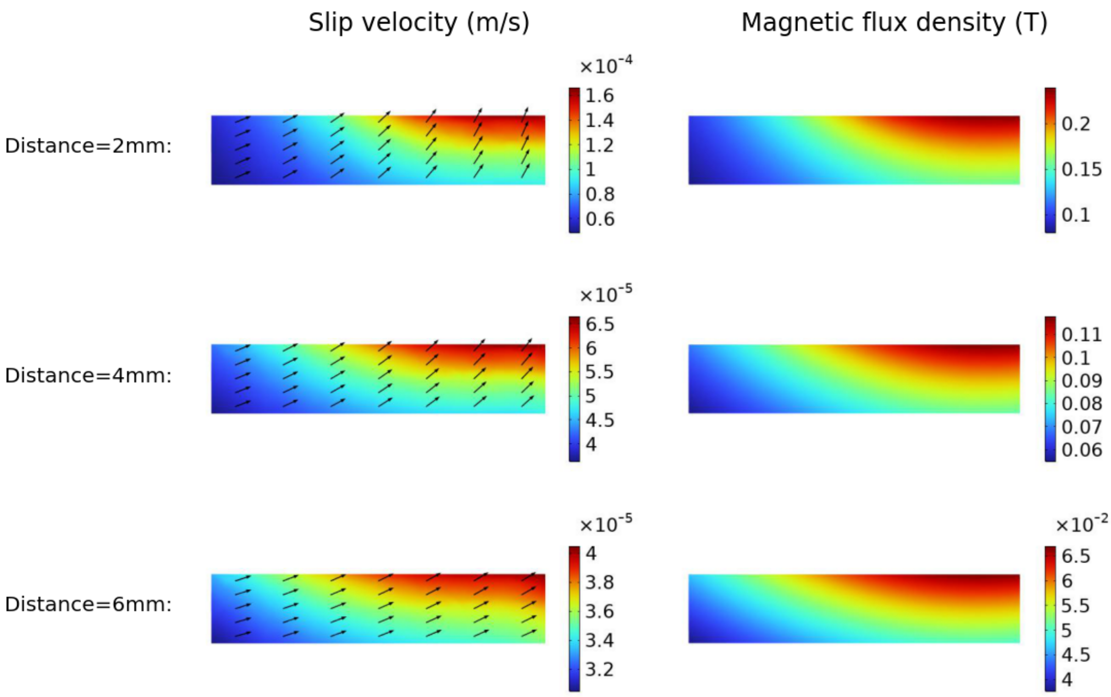

Fig. S 7: Left: Slip velocities and right magnetic flux densities in the collection chamber cross section for different permanent magnet distances to the fluid using the magnet configuration 1.

References

[1] D. T. Grob, N. Wise, O. Oduwole, and S. Sheard, *Magnetic susceptibility characterisation of superparamagnetic microspheres*, Journal of Magnetism and Magnetic Materials, **452**, 134–140 (2018).

[2] P. J. Cregg, K. Murphy, and A. Mardinoglu, *Inclusion of interactions in mathematical modelling of implant-assisted magnetic drug targeting*, Applied Mathematical Modelling, **36**(1), 1–34 (2012).